Frontiers in Bioscience Landmark

Front. Biosci. (Landmark Ed) **2025**; 30(11): 46410
https://doi.org/10.31083/FBL46410

Original Research

Combined Schisandrin B and Temozolomide Treatment Induces Mitochondrial Apoptosis in Glioma Cells

Zebo Tang[1,2], Chaoran Guo[2], Na Wen[2], Hong Jin[2], Yuan Dong[2], Bo Xu[2], Xiangyu Ma[2], Liu Han[3], Jianxin Liu[1,*]

[1]Institute of Neuroscience, Translational Medicine Institute, Xi'an Jiaotong University Health Science Center, 132013 Xi'an, Shaanxi, China
[2]College of Basic Medical Sciences, Jilin Medical University, 132013 Jilin, Jilin, China
[3]College of Pharmacy, Jilin Medical University, 132013 Jilin, Jilin, China
*Correspondence: liujianxin@mail.xjtu.edu.cn (Jianxin Liu)
Academic Editor: Antoni Camins
Submitted: 8 September 2025 Revised: 23 October 2025 Accepted: 31 October 2025 Published: 27 November 2025

Abstract

Background: Temozolomide (TMZ) is a standard chemotherapeutic agent for glioma, but prolonged use frequently leads to drug resistance, reducing its therapeutic efficacy. Schisandrin B (Sch B), a lignan isolated from Schisandra chinensis, demonstrates promising anti-neoplastic activity. This study investigated the synergistic effects of Sch B and TMZ on U87 glioma cells to explore their combined influence on cell viability, apoptosis, and mitochondrial function. **Methods**: U87 glioma cells were treated with Sch B, TMZ, or their combination. Cell viability was assessed using MTT assays. Apoptosis was evaluated by Hoechst staining and flow cytometry, while JC-1 staining and Western blotting were used to assess mitochondrial membrane potential, oxidative stress markers, and apoptosis-related proteins. Cell cycle analysis and pre-treatment with Z-VAD-FMK were performed to confirm pathway involvement. **Results**: Combination treatment significantly reduced cell viability (54.14%) compared to TMZ (72.47%) or Sch B (70.4%) alone. Flow cytometry indicated elevated apoptosis (22.3%) in the combination group. JC-1 staining and protein expression analyses revealed mitochondrial depolarization, cytochrome c release, activation of caspase-3 and -9, and a decreased Bcl-2/Bax ratio. The combined treatment induced G2/M cell cycle arrest via p53/p21 activation and increased oxidative stress. Pre-treatment with Z-VAD-FMK partially reversed these effects, confirming caspase-dependent mitochondrial apoptosis. **Conclusions**: Sch B enhances TMZ-induced cytotoxicity in U87 glioma cells by promoting mitochondrial dysfunction, oxidative stress, and caspase-mediated apoptosis. These findings suggest that Sch B may serve as a promising adjuvant to improve the efficacy of TMZ-based glioma therapy, warranting further validation in resistant and *in-vivo* models.

Keywords: Sch B; TMZ; mitochondrial apoptosis; drug resistance; glioblastoma

1. Introduction

Gliomas represent a primary category of primary brain tumors arising from glial cells. This diverse group of tumors can also arise in the spinal cord. They represent the most common primary malignancy of the central nervous system, comprising nearly 45% of all intracranial tumors [1]. Gliomas exhibit a spectrum of adverse clinical features, including aggressive proliferation, diffuse brain tissue infiltration, high incidence-to-mortality ratios, and a strong propensity for recurrence, which collectively result in a poor prognosis [1]. A recent study of gliomas reported an incidence of 6 cases per 100,000 individuals per year in the United States [2]. In comparison, an earlier study showed the incidence of primary brain tumors in China was 22.52 per 100,000, with gliomas comprising 31.1% of these cases [3]. According to global cancer burden statistics, the incidence of malignant tumors has been rising steadily in recent years, with malignant gliomas representing one of the most rapidly increasing categories among central nervous system tumors [4]. The most common treatment procedure for glioma involves surgical excision integrated with postoperative chemotherapy and radiotherapy. Chemotherapy has proven to be effective as part of this comprehensive management of glioma. Notably, Temozolomide (TMZ) is extensively utilized chemotherapeutic agents in the treatment of gliomas. While TMZ is effective during the initial stages of treatment, glioma cells often develop resistance over time, leading to decreased sensitivity in the intermediate and later stages of malignancy [1]. Therefore, the development of effective strategies to control or treat glioma remains an urgent and ongoing challenge in neuro-oncology.

This widespread use of TMZ for the treatment of glioma is largely due to of its superior oral bioavailability and its capacity to move across the blood-brain-barrier [5]. Numerous studies have demonstrated the effectiveness of TMZ in the treatment of brain gliomas. Furthermore, TMZ has shown therapeutic benefits for both newly diagnosed and relapsed glioblastoma multiforme (GBM) [5] and is a critical treatment option for extending patient survival. While many studies have established its effectiveness, TMZ is not without limitations, including significant toxic side effects such as thrombocytopenia, neutropenia, and lym-

phopenia. Most importantly, drug resistance remains a major concern, highlighting the need for strategies to improve its efficacy while minimizing toxicity and overcoming resistance [5].

In addition to standard chemotherapeutic drugs, growing exploration has been directed toward natural compounds as alternative or complementary approaches for various cancers. Among these, several plant-derived compounds exhibit a wide range of pharmacological properties, most notably their ability to inhibit tumor cell growth and proliferation, making them valuable in cancer therapy [6]. One such compound, Schisandrin B (Sch B), is a bioactive lignan derived from Schisandra chinensis. Sch B has emerged as a particularly promising candidate [7]. This plant-derived bioactive compound has demonstrated diverse pharmacological capacities including antioxidant, anti-inflammatory, and neuroprotective effects. Sch B has been reported to prevent tumor growth and metastasis [8,9] by inducing the differentiation and apoptosis of tumor cells [10,11]. Sch B has also been reported to reverse multidrug resistance in tumor cells [12], increase sensitivity to other anti-tumor drugs [13], and inhibit tumor angiogenesis [14]. Nonetheless, targeting a single therapeutic pathway is often less effective than combination therapies [15]. In this context, combining plant-derived compounds with conventional chemotherapeutic agents has shown synergistic effects [5]. Therefore, in the present study, we examined the combined use of Sch B and TMZ to improve glioma therapy, providing new insights into their synergistic cytotoxic and pro-apoptotic effects *in vitro*. The underlying mechanisms of apoptosis induced by this combination was investigated, with a focus on mitochondrial dysfunction, oxidative stress, and caspase-dependent pathways.

2. Materials and Methods

2.1 Materials and Instruments

Sch B was bought from Shanghai Yuanye Biotechnology Co., Ltd., and TMZ from Shanghai Maclin Biochemical Technology Co., Ltd. DMEM medium and penicillin/streptomycin mixture were acquired from Sigma (St. Louis, MO, USA). Fetal bovine serum was purchased from Thermo Fisher Technologies (Waltham, MA, USA); The caspase inhibitor Z-VAD-FMK was obtained from MCE (Monmouth Junction, NJ, USA); and Kits for malondialdehyde (MDA), superoxide dismutase (SOD), catalase (CAT), and glutathione (GSH) assays were obtained from Jianjieng Bioengineering Institute of Nanjing (Nanjing, China). The kit for detecting reactive oxygen species (ROS) was bought from Shenyang Wanxiang Biological Co., Ltd., while the BCA protein concentration kit, Hoechst 33258 dye solution, Mitochondrial Permeability Conversion Pore (MPTP) assay kit, Annexin V-FITC PI Apoptosis Kit, mitochondrial membrane Potential (MMP) assay Kit, and cell cycle assay kit, were all purchased from Shanghai Biyuntian Biotechnology Company. Equipment included a 5% CO_2 incubator (ThermoFisher Technology Co., Ltd., Waltham, MA, USA), a fluorescence microscope (Leica TCS SP8, Wetzlar, Germany), a flow cytometer (FACSCalibur, San Jose, CA, USA), a gel imaging system (Tanon 5200, Shanghai Tienang Technology Co., Ltd., Shanghai, China), and a full-wavelength enzyme microscope (Epoch, BioTek, Winooski, VT, USA).

2.2 Cell Lines and Cell Culture

Human astroblastoma U87 cells (ATCC® HTB-14™) were acquired from the American Type Culture Collection and their identity was verified by short tandem repeat (STR) profiling. The cells were maintained in a humidified incubator at 37 °C with 5% CO_2, cultured in high-glucose DMEM supplemented with 10% fetal bovine serum (FBS) and 1% penicillin-streptomycin. Routine mycoplasma testing was performed using the MycoAlert™ Detection Kit (Walkersville, MD, USA), with all tests returning negative. For experimental use, cells were harvested upon reaching the logarithmic growth phase and the resulting cell suspension was seeded into either 6-well or 96-well plates.

2.3 Determination of Oxidative Stress Markers and Assessment of ROS Levels

The concentrations of MDA, SOD, CAT, and GSH in the cell homogenate supernatant were determined with respective assay kits following the kit protocols. ROS levels in U87 cells were assessed using a DCFH-DA (2′, 7′-dichlorofluoroscin diacetate) probe. After adding 5 µL of DCFH-DA (1 µM) fluorescent dye to each well, the cells were incubated in the dark in 30 min at 37 °C, then rinsed twice with phosphate-buffered saline (PBS). ROS generation was detected by fluorescence microscopy (Leica TCS SP8, Wetzlar, Germany).

2.4 Analysis of Mitochondrial Membrane Potential (MMP)

Changes in MMP in U87 cells were assessed with the JC-1 assay kit following the manufacturer's protocol. Briefly, cells seeded in 6-well plates were subjected to drug treatments for 24 h. After being rinsed with PBS, the cells were incubated with the working JC-1 staining solution at 37 °C for 30 minutes. Subsequently, unbound dye was removed by washing with the provided 1× assay buffer. The fluorescence intensity was then visualized and captured using a Leica TCS SP8 fluorescence microscope to determine the MMP alterations.

2.5 Hoechst 33258 Staining for the Asssessment of Nuclear Morphology

To assess nuclear morphological changes in U87 cells, the Hoechst 33258 staining kit was employed. After fixation with 4% paraformaldehyde, cells were subjected to PBS washes and permeabilized in 0.2% Triton X-100. Nuclear staining was subsequently performed by incubating

with Hoechst 33258 (10 µg/mL) for 5 min following an additional PBS wash. The stained cells were then observed under a fluorescence microscope (Leica TCS SP8), with bright blue fluorescence indicating the cell nuclei. Quantitative analysis of the images was performed using Image pro plus 6.0 software (Media Cybernetics, Rockville, MD, USA).

2.6 Detection of Annexin V-FITC/PI Apoptosis

The Annexin V-FITC/PI double-staining method was utilized to detect apoptosis. Cells were harvested, washed twice with PBS, and the resulting cell pellet was collected by centrifugation. The culture medium was discarded, and cells were digested with trypsin. After digestion, cells were transferred to a centrifuge tube, washed with PBS, and centrifuged again to obtain a cell pellet. The pellet was then resuspended in buffer, and FITC Annexin V staining solution (green fluorescence) was added. The admixture was gently mixed and incubated in the dark for 5 minutes. Subsequently, the PI staining solution (red fluorescence) was added and incubated for 5 minutes. After staining, PBS was added in a volume appropriate to the cell count, and the proportion of apoptotic cells was analyzed using flow cytometry (FACSCalibur, San Jose, CA, USA).

2.7 Detection of Mitochondrial Permeability Transition Pore (MPTP)

The culture medium was aspirated from the 6-well plate. Cultures were supplemented with Calcein AM and the corresponding fluorescence quenching reagent at specified volumes, following the MPTP detection kit guidelines. Following a 45 min incubation at 37 °C in the dark, the staining solution was exchanged for fresh pre-warmed culture medium and the cells were incubated for an additional 30 min under identical conditions. Removed the medium and rinsed the wells 2–3 times with PBS. Detection buffer was then added before observation under a fluorescence microscope.

2.8 Assessment of Cell Cycle by Flow Cytometry

After centrifugation and PBS resuspension, cells were subsequently fixed through incubation in 1 mL of pre-cooled 70% ethanol for 2 h at 4 °C, as directed by the Cell Cycle and Apoptosis Detection Kit. Following fixation, the cells were centrifuged, and the pellet was collected. Each sample was then resuspended in 0.5 mL of propidium iodide (PI) staining solution and incubated in a water bath at 37 °C for 30 min in the dark. Samples were analyzed by flow cytometry using a 488-nm excitation wavelength.

2.9 MTT-Based Evaluation of U87 Cell Proliferation

Cells were allocated into four experimental groups: control, TMZ treated, Sch B treated, and TMZ + Sch B co-treated. Each group was allocated five wells. After treatment, cells were plated in 96-well plates at 6×10^4 cells/well. After adding 10 µL MTT solution per well, the plates were incubated for 2 h. The absorbance of each well was subsequently determined at 450 nm using a microplate reader.

2.10 Western Blot Analysis

U87 cells were lysed for 2 h, and the protein concentration was measured using a BCA assay kit. The protein lysate was boiled at 100 °C for 7 min for denaturation. The samples were resolved by SDS-PAGE and subsequently transferred to a PVDF membrane. The membrane was then blocked with 5% non-fat milk for 2 h. Primary antibodies were incubated with the membrane at 4 °C overnight to detect proteins of interest: Cytochrome c (1:1000, 66264-1-IG, Proteintech, Wuhan, China), Bax (1:4000, 50599-2-ig, Proteintech), (cleaved)-Caspase E9 (1:1000, 66169-1-ig, Proteintech), Bcl-xL (1:100,000, 10773-1-AP, Proteintech), Bcl-2 (1:4000, 68103-1-ig, Proteintech), cleaved-caspase3 (1:10,000, 82202-1-RR, Proteintech), CDK4 (1:4000, 11026-1AP, Proteintech), P21 (1:2000, 10355-1-AP, Proteintech), P53 (1:10,000, 60283-2-IG, Proteintech), and GAPDH (1:50,000, 60004-1 1-Ig, Proteintech). Following the incubation period, the membrane was rinsed with TBST to remove unbound antibodies. Subsequently, it was probed with the corresponding HRP-conjugated secondary antibody for 1 h. The protein bands were colored using Emitter Coupled Logic (ECL) and analyzed by Image pro plus 6.0 software (Media Cybernetics, Rockville, MD, USA).

2.11 Statistical Analysis

Statistical analyses were conducted with GraphPad Prism 8.0.4 (GraphPad Software, San Diego, CA, USA). All experiments included three independent biological replicates (n = 3) with triple technical replicates per condition. Data are presented as mean ± standard deviation (SD). Group comparisons were performed using unpaired two-tailed Student's *t*-test (two groups) or one-way ANOVA with Tukey's post-hoc test (multiple groups). Significance levels are indicated as $*p < 0.05$, $**p < 0.01$, and $***p < 0.001$.

3. Results

3.1 Anti-Proliferative Effect of TMZ Combined With Sch B on U87 Cells

The effects of TMZ, Sch B, and their combination on U87 cell proliferation were analyzed using an MTT assay. Varying doses of TMZ, Sch B and TMZ + Sch B were used to treat cells for 48 h followed by MTT incubation to evaluate cell viability. TMZ (0–400 µM) exerted a dose-dependent inhibitory effect on U87 cell proliferation (Fig. 1A). At a concentration of 200 µM, TMZ reduced U87 cell viability to 72.47% compared to the control group. Similarly, Sch B suppressed U87 cell proliferation over a concentration range of 0–1600 µg/mL (Fig. 1B), reducing

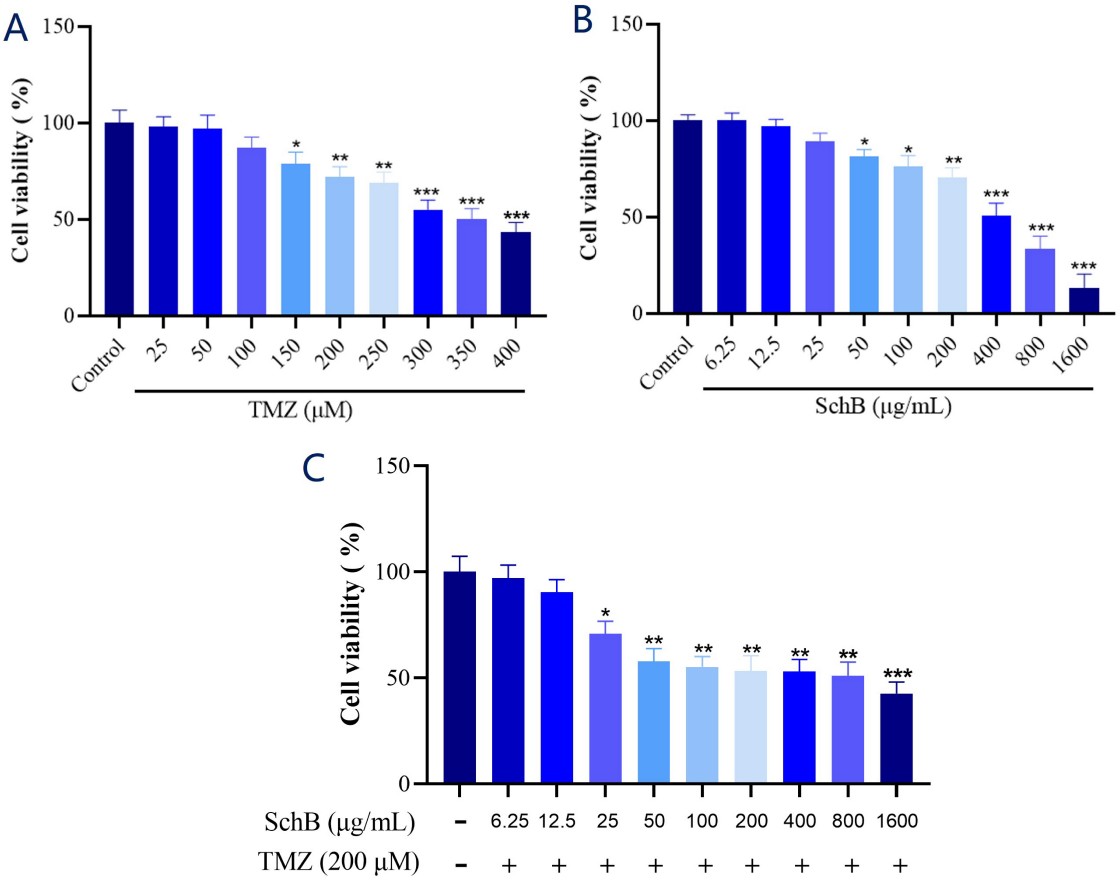

Fig. 1. Cell viability was assessed by MTT assay. (A) Effects of TMZ on U87 cell viability. (B) Effects of Sch B on U87 cell viability. (C) Effects of TMZ and Sch B combination on U87 cell viability. Data are presented as mean ± SD. Statistical significance is denoted as follows: $*p < 0.05$, $**p < 0.01$, $***p < 0.0001$. TMZ, Temozolomide; Sch B, Schisandrin B.

cell viability to 70.4% at 200 μg/mL. When a constant concentration of TMZ (200 μM) was combined with increasing concentrations Sch B, U87 cell viability further de-creased (Fig. 1C). Notably, the combination of 200 μM TMZ and 200 μg/mL Sch B reduced U87 cell viability to 54.14%, producing a more pronounced inhibitory effect than either agent alone, which suggests a synergistic effect between Sch B and TMZ.

3.2 Effect of TMZ and Sch B Combination on U87 Cell Apoptosis

Hoechst staining showed that the integration of TMZ and Sch B resulted in significantly brighter blue fluorescence compared to either treatment alone, indicating enhanced apoptosis in U87 cells (Fig. 2A). Flow cytometry further confirmed the enhanced apoptosis induced by the combined treatment (Fig. 2B). Western blot indicated that the combination treatment modulated the expression of key apoptotic regulators relative to single-agent treatments. Specifically, it elevated pro-apoptotic proteins (Bax, cytochrome c) while reducing anti-apoptotic proteins (Bcl-2, Bcl-xL). This shift in the balance was accompanied by activation of caspase-3 and caspase-9, thereby promoting apoptosis in U87 cells (Fig. 2C). Additionally, JC-1 staining showed a reduction in the red/green fluorescence ratio, suggesting a decrement in the MMP. While both TMZ and Sch B individually caused a decline in mitochondrial membrane potential, their combination led to a more pronounced effect, further accelerating apoptosis in U87 cells (Fig. 2D). These results suggest that TMZ and Sch B act synergistically to enhance apoptotic signaling in glioma cells, likely through amplification of the intrinsic mitochondrial pathway. This combination may provide a promising therapeutic approach for glioblastoma by improving treatment efficacy and potentially overcoming resistance to standard chemotherapy.

3.3 Effect of TMZ and Sch B Combination on Mitochondrial Function in U87 Cells

Mitochondrion acts as a key regulator of the intrinsic apoptotic pathway. The maintenance of mitochondrial integrity is largely influenced by the MPTP, a non-selective channel connecting the inner and outer mitochondrial membranes, whose opening permits the release of pro-apoptotic factors that drive cell death. In this study, MPTP staining revealed that treatment with either TMZ or Sch B resulted

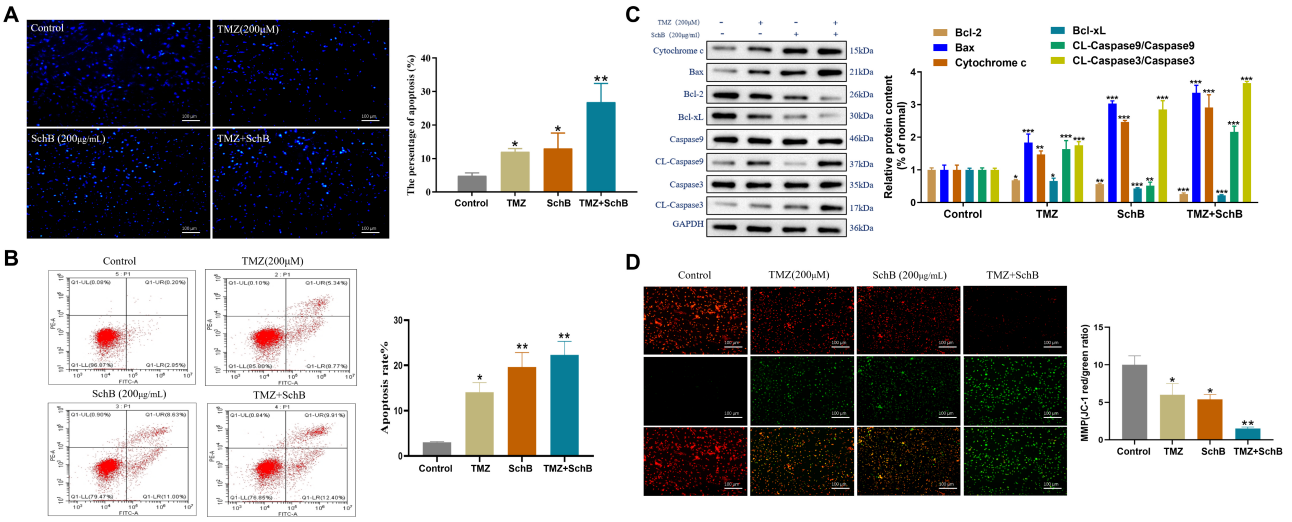

Fig. 2. Effect of TMZ and Sch B combination on U87 cell apoptosis. (A) Hoechst 33342 staining shows condensed and fragmented nuclei indicating apoptosis. Scale bar = 100 μm. (B) Flow cytometric analysis quantifies apoptotic cells. (C) Analysis of apoptosis-related protein expression by Western blot. (D) Detection of mitochondrial membrane potential changes by JC-1 staining. Scale bar = 100 μm. Data are presented as mean ± SD (n = 3). Statistical significance is reported at $*p < 0.05$, $**p < 0.01$, and $***p < 0.001$.

in moderate pore opening, as indicated by de-creased green fluorescence. However, the combination treatment of TMZ and Sch B led to a more pronounced loss of fluorescence, suggesting a significant increase in opening of the MPTP (Fig. 3A). Sustained MPTP opening is known to trigger mitochondrial oxidative stress by increasing the level of reactive oxygen species (ROS) accumulation. Staining for ROS revealed a marked rise in level of intra-cellular ROS following the pretreatment of TMZ and Sch B, as evidenced by enhanced green fluorescence (Fig. 3B). This result indicates an aggravation of oxidative stress. Notably, the combination group exhibited a marked increase in MDA levels, an indicator of lipid peroxidation, relative to the individual treatments, suggesting severe mitochondrial membrane impairment (Fig. 3C).

To further evaluate the redox status, the levels of key intracellular antioxidants such as SOD, CAT, and reduced GSH were measured. A substantial decline in these antioxidant defenses was observed in the combination treatment group, indicating compromised antioxidant capacity and a shift toward a pro-oxidant state (Fig. 3D–F). Together, our data indicate that the TMZ/Sch B enhances mitochondrial dysfunction through increased MPTP opening, elevated ROS production, and impaired antioxidant defense, thereby amplifying oxidative stress-mediated apoptosis in glioma U87 cells.

3.4 TMZ and Sch B Combination Induces G2/M Cell Cycle Arrest in U87 Cells

Cyclin-dependent kinase 4 (CDK4) is important for regulating the G1 to S phase transition during cell-cycle progression. In response to DNA impairment, the tumor suppressor protein p53 promotes transcription of the CDK inhibitor p21, which subsequently inhibits CDK activity and halts progression of cell cycle. Western blot analysis revealed that combined treatment with TMZ and Sch B significantly reduced CDK4 expression and upregulated p53 and p21 levels when compared with controls, indicating disruption of normal cell cycle regulation (Fig. 4A) ($p < 0.05$). Flow cytometric detection showed that TMZ + Sch B caused notable arrest of U87 cells at the G2/M transition, indicating effective cell cycle blockade at this phase (Fig. 4B).

3.5 Z-VAD-FMK Attenuates TMZ/Sch B-Induced Apoptosis in U87 Cells

Z-VAD-FMK, a broad-spectrum and cell-permeable caspase inhibitor, is widely used to block caspase-dependent apoptosis. To verify whether TMZ + Sch B-induced cell death in U87 cells occurs through a caspase-dependent pathway, cells were pretreated with Z-VAD-FMK before combination treatment. Hoechst 33342 staining (Fig. 5A) confirmed the inhibitory effect of Z-VAD-FMK on apoptosis, showing fewer condensed nuclei and reduced bright-blue fluorescence in the TMZ + Sch B + Z-VAD-FMK group compared with the TMZ + Sch B group. Flow-cytometric analysis (Fig. 5B) supported these findings, showing that the apoptotic rate increased to 19.3% following TMZ + Sch B treatment but decreased to 13.8% after Z-VAD-FMK co-treatment, confirming that the inhibitor effectively reduced combination-induced apoptosis. Western blot analysis (Fig. 5C) showed that Z-VAD-FMK increased anti-apoptotic protein Bcl-2 while reducing pro-apoptotic markers (Bax, cytochrome c, cleaved caspase-9, and cleaved caspase-3), indicating suppression of caspase activation. JC-1 staining (Fig. 5D) demonstrated

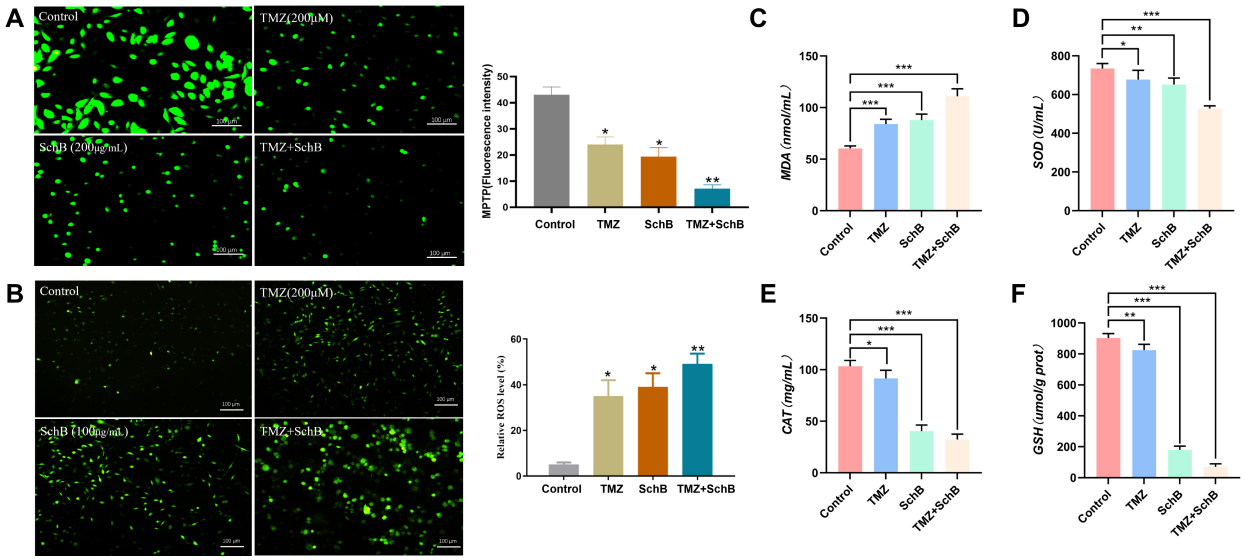

Fig. 3. Effect of TMZ/Sch B combination on the mitochondrial function of U87 cells. (A) MPTP staining evaluates mitochondrial permeability transition pore opening. Scale bar = 100 μm. (B) ROS levels measured by DCFH-DA staining. Scale bar = 100 μm. (C) Lipid peroxidation assessed via MDA content. (D–F) Antioxidant enzyme activities of SOD, CAT, and GSH, respectively. Data are presented as mean ± SD. *$p < 0.05$, **$p < 0.01$, and ***$p < 0.001$. MPTP, Mitochondrial Permeability Conversion Pore; ROS, reactive oxygen species; SOD, superoxide dismutase; CAT, catalase; GSH, glutathione.

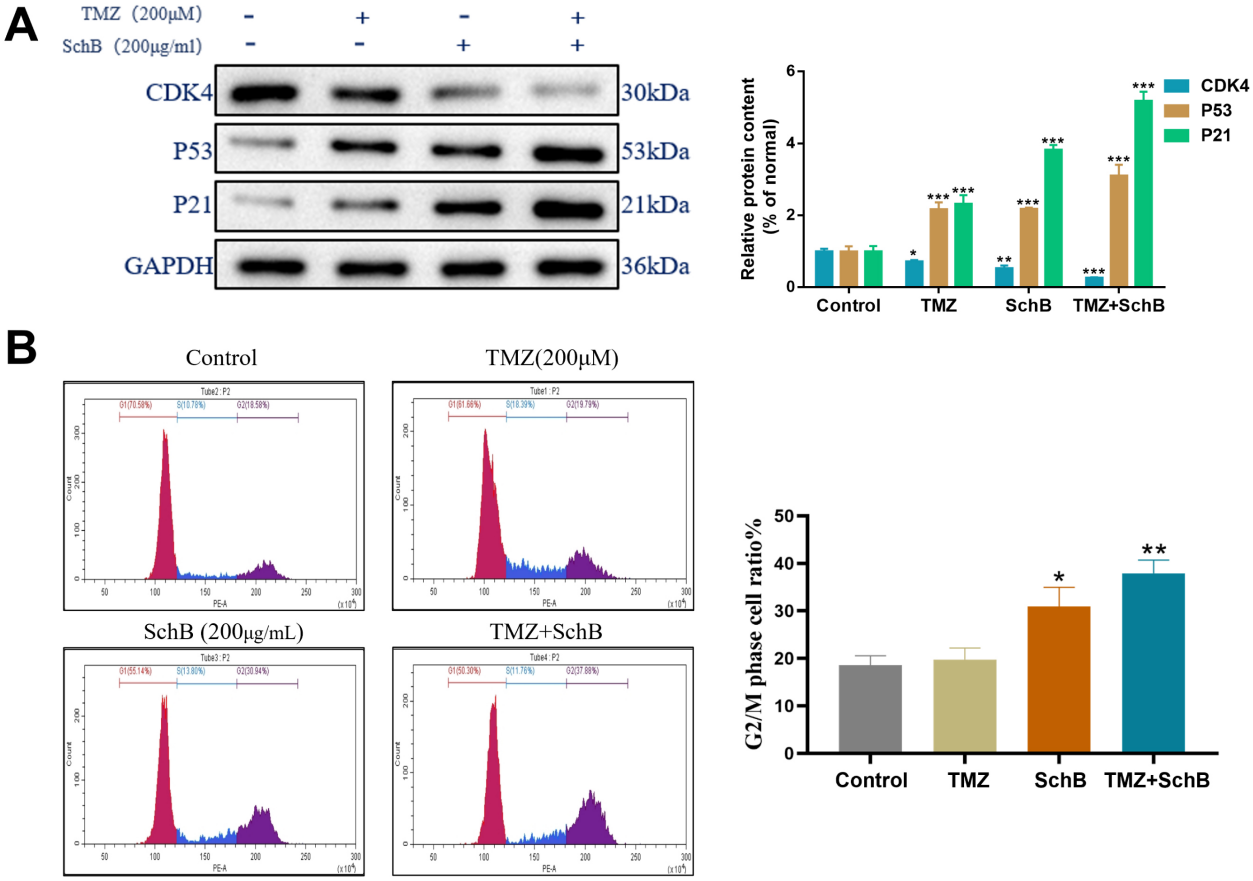

Fig. 4. Effect of TMZ/Sch B on the U87 cell cycle. (A) Western blot analysis of CDK4, p53, and p21 protein expression. (B) Flow cytometry of DNA content showing changes in cell cycle phases. Quantification based on triplicate experiments, *$p < 0.05$, **$p < 0.01$, and ***$p < 0.001$.

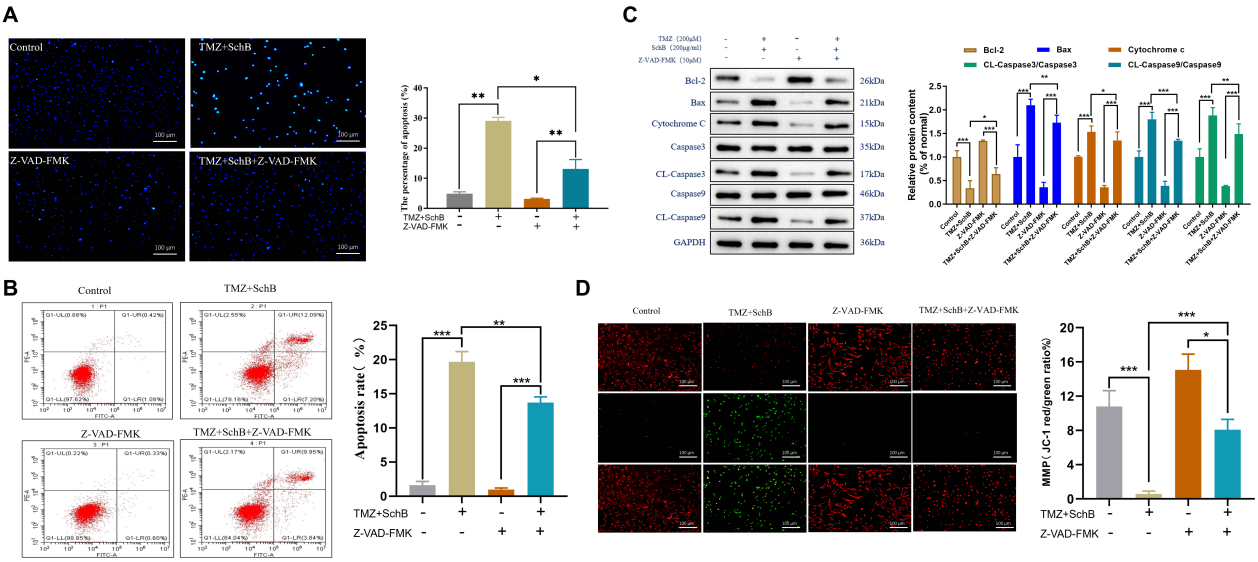

Fig. 5. Effects of Z-VAD-FMK on apoptosis in U87 cells induced by TMZ and Sch B. (A) Hoechst staining reveals nuclear changes. Scale bar = 100 μm. (B) Flow cytometry quantifies apoptotic rate. (C) Western blot showing caspase activation. (D) JC-1 staining visualizes mitochondrial potential restoration by Z-VAD-FMK. Scale bar = 100 μm. Data shown as mean ± SD (n = 3). *$p < 0.05$, **$p < 0.01$, and ***$p < 0.001$.

that TMZ + Sch B treatment caused a pronounced loss of mitochondrial membrane potential (MMP), whereas co-treatment with Z-VAD-FMK partially restored MMP, as indicated by an elevated red/green fluorescence ratio. Collectively, these results demonstrate that TMZ + Sch B induces caspase-dependent apoptosis in U87 cells, which can be partially reversed by Z-VAD-FMK.

3.6 Z-VAD-FMK Reverses Mitochondrial Damage Induced by TMZ and Sch B in U87 Cells

To assess the role of caspase inhibition in mitigating mitochondrial dysfunction, U87 cells were co-treated with Z-VAD-FMK alongside TMZ and Sch B. MPTP staining demonstrated increased green fluorescence in the presence of Z-VAD-FMK compared to the TMZ + Sch B group alone, indicating reduced MPTP opening and improved mitochondrial integrity (Fig. 6A). Similarly, ROS staining revealed diminished green fluorescence following Z-VAD-FMK treatment, indicating a significant reduction of intracellular ROS and alleviation of oxidative stress (Fig. 6B). Lipid peroxidation, assessed via MDA levels, was significantly lower in the Z-VAD-FMK-treated group compared to cells treated with TMZ + Sch B alone, indicating reduced mitochondrial membrane damage (Fig. 6C). Moreover, the levels of key intracellular antioxidants (SOD, CAT, and GSH) were significantly elevated in the Z-VAD-FMK co-treatment group, reflecting enhanced antioxidant defense and restoration of mitochondrial function (Fig. 6D–F).

4. Discussion

As the most common primary malignant tumor in the central nervous system, GBM exhibits extremely strong invasive characteristics. Despite extensive research efforts, the prognosis for GBM remains poor [16]. TMZ is currently the only approved chemotherapy for GBM; however, most patients eventually develop resistance [17]. Evidence from prior research indicates that Sch B suppresses the proliferation of U87 glioma cells, exhibiting clear dependence on both concentration and exposure duration [18,19]. In the present study, the combination of Sch B and TMZ significantly suppressed U87 cell proliferation, reduced MMP, induced mitochondrial dysfunction, and caused cell cycle arrest at the G2/M phase. These effects collectively led to mitochondria-dependent apoptosis in U87 cells. Excessive oxidative stress, which compromises the body's defense mechanisms, contributes to the pathogenesis of various human diseases, particularly cancer. Elevated ROS levels induce cellular and tissue damage, thereby fostering a microenvironment conducive to tumorigenesis [20]. ROS are primarily generated in the mitochondria and can harm cellular components, ultimately leading to cell death under oxidative stress conditions [21]. In the current study, treatment with Sch B + TMZ increased the levels of MDA and ROS, while simultaneously lowering the levels of antioxidants, such as SOD, CAT, and GSH. These changes indicate a diminished capacity of U87 cells to resist oxidative damage in the presence of Sch B and TMZ.

The p53 protein plays a fundamental role in tumor suppression and represents one of the most frequent mutational targets across human malignancies [22,23]. Under cellular stress, p53 is activated and functions as a transcription factor, leading to cell cycle arrest and apoptosis [24]. p21, a CDK inhibitor, contributes to cell cycle arrest by binding to CDK1, CDK2, and CDK4/6 [25]. In response to cellular

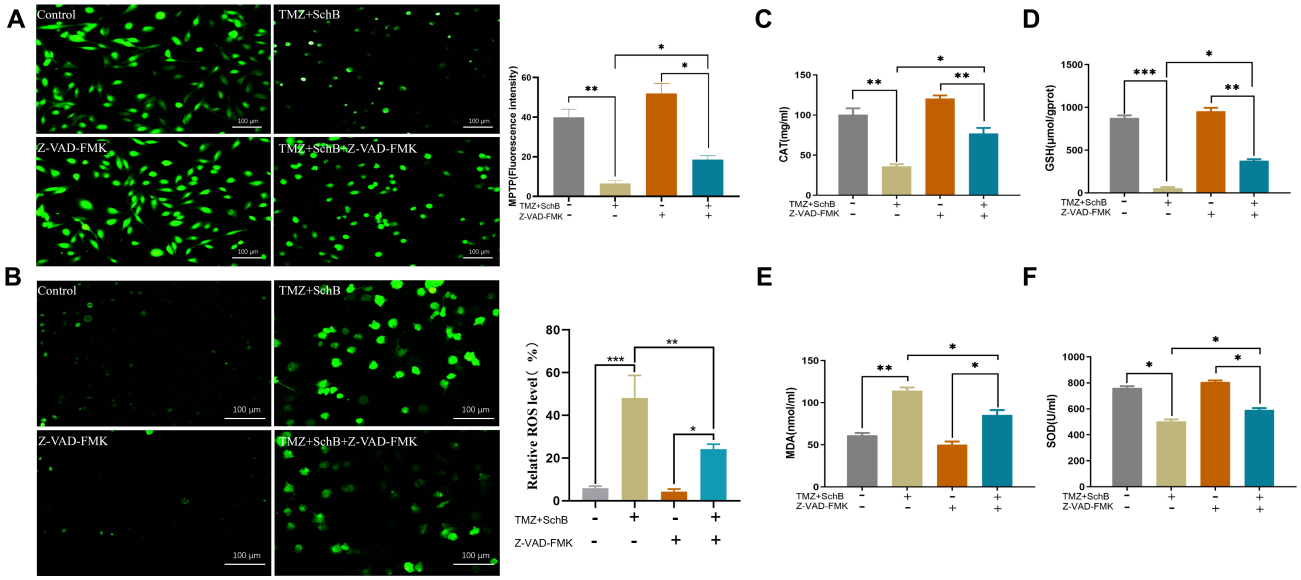

Fig. 6. Effects of Z-VAD-FMK on mitochondrial function in U87 cells treated with TMZ and Sch B. (A) MPTP. Scale bar = 100 μm. (B) ROS. Scale bar = 100 μm. (C) MDA. (D) SOD. (E) CAT. (F) GSH levels were measured to assess mitochondrial damage and oxidative stress. Z-VAD-FMK reduced oxidative markers and restored antioxidant enzyme levels. *$p < 0.05$, **$p < 0.01$, and ***$p < 0.001$ indicates statistical significance.

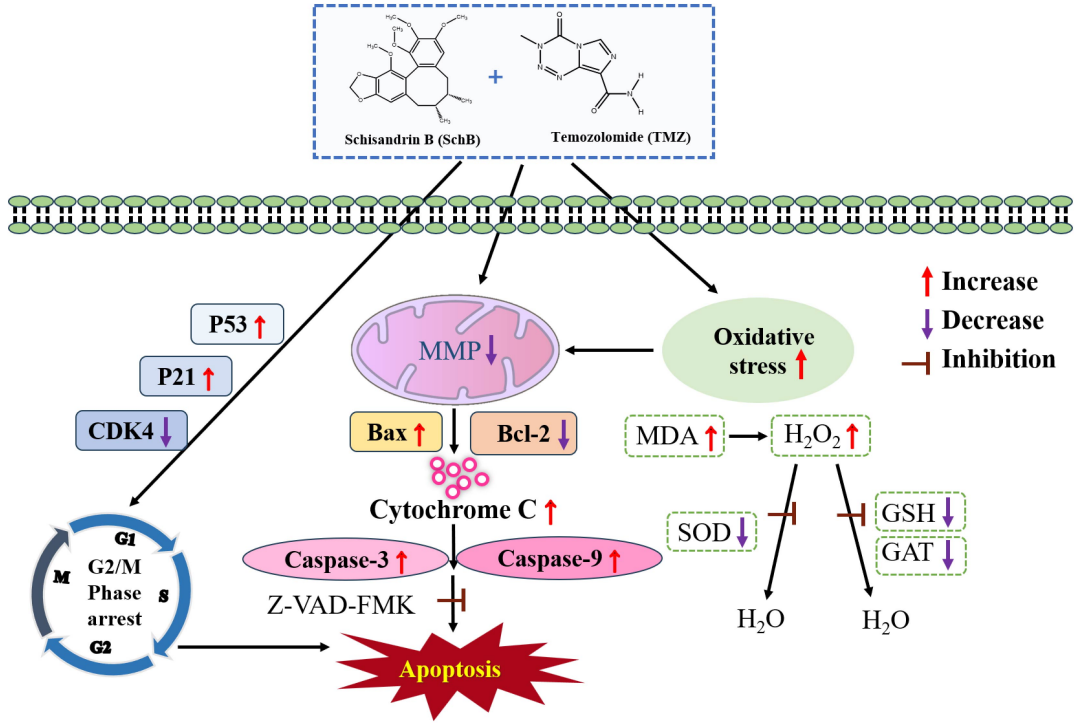

Fig. 7. Proposed mechanism of apoptosis induced by combined Sch B and TMZ treatment of U87 glioma cells. The schematic diagram illustrates activation of the mitochondrial apoptosis pathway through ROS production, mitochondrial dysfunction, and caspase activation in response to the TMZ and Sch B combination. This model is based on the molecular and biochemical changes observed across experiments. MMP, mitochondrial membrane potential.

damage, p53 activation promotes cell growth arrest. p21 is strongly induced by p53, thereby playing a key role in this process [26–28]. In the present study, the combination of Sch B and TMZ activated the p53–p21 pathway, consequently inducing G2/M phase cell cycle arrest. These findings indicate that Sch B + TMZ inhibits U87 glioma cell

proliferation through p53/p21-mediated cell cycle arrest.

Cell apoptosis is a key mechanism through which many anticancer drugs exert their effects, with the mitochondrial pathway being one of the primary routes for inducing tumor cell apoptosis (Fig. 7). Previous research has shown that the caspase family and Bcl-2 proteins play essential roles in regulating this process [29–31]. The Bcl-2 protein family comprises pro-apoptotic members such as Bax and anti-apoptotic members including Bcl-2, serving as pivotal regulators of mitochondrial apoptosis [32–34]. A low Bcl-2/Bax ratio disrupts the MMP, triggers cytochrome c release, and initiates apoptosis [35]. In our study, Sch B and TMZ combination activated caspase-3 and caspase-9 and increased the release of cytochrome c. Compared to the control group, the Bcl-2/Bax ratio was significantly reduced following Sch B + TMZ treatment, along with a substantial decrease in mitochondrial membrane potential in U87 cells. These findings indicate that the Sch B + TMZ combination promotes the apoptotic process in U87 cells.

Caspase participation was examined by Z-VAD-FMK-mediated inhibition coupled with cell viability assessment. Flow cytometry showed that the combination of Sch B/TMZ significantly increased the cell apoptosis rate, but the percentage of cell necrosis did not change significantly after the addition of Z-VAD-FMK inhibitor. However, the proportion of viable cells increased significantly, confirming that apoptosis was the primary mode of cell death induced by Sch B + TMZ. This was further supported by Western blot analysis, as the addition of Z-VAD-FMK effectively blocked caspase-3 activation, elevated the Bcl-2/Bax ratio while suppressing cytochrome c release. These findings imply the Sch B + TMZ combination induces apoptosis through a mitochondria-dependent pathway mediated by caspase activation and Bax upregulation. Therefore, these data demonstrate that the Sch B-TMZ combination activates the mitochondrial apoptotic pathway in U87 glioma cells, irrespective of Z-VAD-FMK co-treatment (Fig. 7). Although Sch B shows promising anti-glioma activity *in vitro*, its clinical application is limited by poor bioavailability and uncertain penetration of the blood-brain barrier (BBB). As a lipophilic compound with low aqueous solubility, Sch B may have limited systemic distribution. Advanced delivery systems, such as lipid-based nanoparticles or surface-modified liposomes, could potentially enhance its BBB permeability and therapeutic efficacy. Future studies should explore such formulations in order to optimize the pharmacokinetic and pharmacodynamic properties of Sch B in glioma therapy.

Study Limitations

This study was conducted exclusively using the U87 glioma cell line. Although well-characterized, these cells may not fully represent the molecular and phenotypic diversity of glioblastoma. Consequently, the results should be interpreted as preliminary evidence of synergistic and pro-apoptotic effects *in vitro*, rather than as confirmation of resistance reversal. In addition, quantitative assessment of the synergistic interaction (e.g., using a Chou–Talalay synergy index) was not performed and should be included in future studies to substantiate the combined effect. Future investigations that incorporate additional glioma cell lines (e.g., T98G, U251, and LN229) and patient-derived primary cultures will be essential to validate these findings across diverse tumor backgrounds. Moreover, *in-vivo* studies with xenograft or orthotopic glioma models are needed to evaluate pharmacokinetic interactions, tumor microenvironment effects, and systemic safety of the Sch B + TMZ combination. Despite these limitations, the current work provides a mechanistic foundation that supports the potential of Sch B as an adjunct agent to enhance TMZ efficacy in glioma therapy.

5. Conclusions

In the current study, the combination of Sch B and TMZ exhibited synergistic anti-tumor effects against U87 glioma cells by inducing mitochondria-mediated, caspase-dependent apoptosis. The treatment enhanced oxidative stress, disrupted MMP, and activated Bax, cytochrome c, and cleaved caspase-3/-9, while promoting G2/M cell cycle arrest via the p53/p21 pathway and suppression of CDK4. The attenuation of these effects by Z-VAD-FMK confirmed the involvement of the intrinsic apoptotic pathway. However, possible participation of non-apoptotic mechanisms such as necroptosis warrants further exploration. Future *in vivo* studies using TMZ-resistant and MGMT-high glioma models are needed to validate the therapeutic potential, pharmacokinetics, and safety of Sch B + TMZ treatment.

Availability of Data and Materials

The datasets used and analyzed during the current study are available from the corresponding author on reasonable request.

Author Contributions

Investigation, Methodology, Data curation, Validation, Formal analysis, Writing—original draft, Writing—review & editing, ZT; Methodology, Validation, Formal analysis, CG; Investigation, Methodology, Formal analysis, NW; Investigation, Methodology, Formal analysis, HJ; Data curation, Investigation, Formal analysis, YD; Investigation, Methodology, Formal analysis, BX; Investigation, Methodology, Formal analysis, XM; Investigation, Methodology, LH; Conceptualization, Methodology, Writing—review & editing, Funding acquisition, JL. All authors contributed to editorial changes in the manuscript. All authors read and approved the final manuscript. All authors have participated sufficiently in the work and agreed to be accountable for all aspects of the work.

Ethics Approval and Consent to Participate

Not applicable.

Acknowledgment

Not applicable.

Funding

This research was funded by the Jilin province science and technology development plan (YDZJ202101ZYTS095) and Foundation of Innovation and Entrepreneurship Program of college students in Jilin Province (No. 2021005).

Conflict of Interest

The authors declare no conflict of interest.

Declaration of AI and AI-Assisted Technologies in the Writing Process

During the preparation of this work, the authors used Generative AI to check spelling and grammar. After using this tool, the authors reviewed and edited the content as needed and took full responsibility for the content of the publication.

References

[1] Hong X, Zhang J, Zou J, Ouyang J, Xiao B, Wang P, *et al*. Role of COL6A2 in malignant progression and temozolomide resistance of glioma. Cellular Signalling. 2023; 102: 110560. https://doi.org/10.1016/j.cellsig.2022.110560.

[2] Mesfin FB, Karsonovich T, Al-Dhahir MA. Gliomas. In StatPearls. StatPearls Publishing: Treasure Island (FL). 2025.

[3] Zhao Z, Zhang KN, Wang Q, Li G, Zeng F, Zhang Y, *et al*. Chinese Glioma Genome Atlas (CGGA): A Comprehensive Resource with Functional Genomic Data from Chinese Glioma Patients. Genomics, Proteomics & Bioinformatics. 2021; 19: 1-12. https://doi.org/10.1016/j.gpb.2020.10.005.

[4] He J, Yang A, Zhao X, Liu Y, Liu S, Wang D. Anti-colon cancer activity of water-soluble polysaccharides extracted from Gloeostereum incarnatum via Wnt/β-catenin signaling pathway. Food Science and Human Wellness. 2021; 10: 460–470. https://doi.org/10.1016/j.fshw.2021.04.008.

[5] Kundu M, Das S, Nandi S, Dhara D, Mandal M. Magnolol and Temozolomide exhibit a synergistic anti-glioma activity through MGMT inhibition. Biochimica et Biophysica Acta. Molecular Basis of Disease. 2023; 1869: 166782. https://doi.org/10.1016/j.bbadis.2023.166782.

[6] Miao YH, Wang X, Zhao XM, Hu YW, Liu X, Deng DW. Co-assembly strategies of natural plant compounds for improving their bioavailability. Food & Medicine Homology. 2025; 2: 9420022.

[7] Hu JN, Wang YM, Zhang H, Li HP, Wang Z, Han M, *et al*. Schisandra B, a representative lignan from Schisandra chinensis, improves cisplatin-induced toxicity: An in vitro study. Phytotherapy Research. 2023; 37: 658–671. https://doi.org/10.1002/ptr.7644.

[8] Kou X, Kirberger M, Yang Y, Chen N. Natural products for cancer prevention associated with Nrf2–ARE pathway. Food Science and Human Wellness. 2013; 2: 22–28. https://doi.org/10.1016/j.fshw.2013.01.001.

[9] Dai X, Yin C, Guo G, Zhang Y, Zhao C, Qian J, *et al*. Schisandrin B exhibits potent anticancer activity in triple negative breast cancer by inhibiting STAT3. Toxicology and Applied Pharmacology. 2018; 358: 110–119. https://doi.org/10.1016/j.taap.2018.09.005.

[10] Co VA, El-Nezami H, Liu Y, Twum B, Dey P, Cox PA, *et al*. Schisandrin B Suppresses Colon Cancer Growth by Inducing Cell Cycle Arrest and Apoptosis: Molecular Mechanism and Therapeutic Potential. ACS Pharmacology & Translational Science. 2024; 7: 863–877. https://doi.org/10.1021/acsptsci.4c00009.

[11] Lv XJ, Zhao LJ, Hao YQ, Su ZZ, Li JY, Du YW, *et al*. Schisandrin B inhibits the proliferation of human lung adenocarcinoma A549 cells by inducing cycle arrest and apoptosis. International Journal of Clinical and Experimental Medicine. 2015; 8: 6926–6936.

[12] Wang S, Wang A, Shao M, Lin L, Li P, Wang Y. Schisandrin B reverses doxorubicin resistance through inhibiting P-glycoprotein and promoting proteasome-mediated degradation of survivin. Scientific Reports. 2017; 7: 8419. https://doi.org/10.1038/s41598-017-08817-x.

[13] Jin J, Bi H, Hu J, Zhong G, Zhao L, Huang Z, *et al*. Enhancement of oral bioavailability of paclitaxel after oral administration of Schisandrol B in rats. Biopharmaceutics & Drug disposition. 2010; 31: 264-8. https://doi.org/10.1002/bdd.705.

[14] Zhang L, Kong L, He SY, Liu XZ, Liu Y, Zang J, *et al*. The anti-ovarian cancer effect of RPV modified paclitaxel plus schisandra B liposomes in SK-OV-3 cells and tumor-bearing mice. Life Sciences. 2021; 285: 120013. https://doi.org/10.1016/j.lfs.2021.120013.

[15] Wang J, Liao ZX. Research progress of microrobots in tumor drug delivery. Food & Medicine Homology. 2024; 1: 9420025.

[16] Lau D, Magill ST, Aghi MK. Molecularly targeted therapies for recurrent glioblastoma: current and future targets. Neurosurgical Focus. 2014; 37: E15. https://doi.org/10.3171/2014.9.FOCUS14519.

[17] Maghrouni A, Givari M, Jalili-Nik M, Mollazadeh H, Bibak B, Sadeghi MM, *et al*. Targeting the PD-1/PD-L1 pathway in glioblastoma multiforme: Preclinical evidence and clinical interventions. International Immunopharmacology. 2021; 93: 107403. https://doi.org/10.1016/j.intimp.2021.107403.

[18] Jiang Y, Zhang Q, Bao J, Du C, Wang J, Tong Q, *et al*. Schisandrin B suppresses glioma cell metastasis mediated by inhibition of mTOR/MMP-9 signal pathway. Biomedicine & Pharmacotherapy. 2015; 74: 77–82. https://doi.org/10.1016/j.biopha.2015.07.006.

[19] Li Q, Lu XH, Wang CD, Cai L, Lu JL, Wu JS, *et al*. Antiproliferative and apoptosis-inducing activity of schisandrin B against human glioma cells. Cancer Cell International. 2015; 15: 12. https://doi.org/10.1186/s12935-015-0160-x.

[20] Li X, Hou Y, Zhao J, Li J, Wang S, Fang J. Combination of chemotherapy and oxidative stress to enhance cancer cell apoptosis. Chemical Science. 2020; 11: 3215–3222. https://doi.org/10.1039/c9sc05997k.

[21] Ray PD, Huang BW, Tsuji Y. Reactive oxygen species (ROS) homeostasis and redox regulation in cellular signaling. Cellular Signalling. 2012; 24: 981–990. https://doi.org/10.1016/j.cellsig.2012.01.008.

[22] Liu J, Zhang C, Hu W, Feng Z. Tumor suppressor p53 and its mutants in cancer metabolism. Cancer Letters. 2015; 356: 197-203. https://doi.org/10.1016/j.canlet.2013.12.025.

[23] Boutelle AM, Attardi LD. p53 and Tumor Suppression: It Takes a Network. Trends in Cell Biology. 2021; 31: 298–310. https://doi.org/10.1016/j.tcb.2020.12.011.

[24] Pflaum J, Schlosser S, Müller M. p53 Family and Cellular Stress Responses in Cancer. Frontiers in Oncology. 2014; 4: 285. https://doi.org/10.3389/fonc.2014.00285.

[25] Leontieva OV, Blagosklonny MV. CDK4/6-inhibiting drug substitutes for p21 and p16 in senescence: duration of cell cycle arrest and MTOR activity determine geroconversion. Cell Cycle. 2013; 12: 3063–3069. https://doi.org/10.4161/cc.26130.

[26] Cullot G, Boutin J, Fayet S, Prat F, Rosier J, Cappellen D, *et al*. Cell cycle arrest and p53 prevent ON-target megabase-scale rearrangements induced by CRISPR-Cas9. Nature Communications. 2023; 14: 4072. https://doi.org/10.1038/s41467-023-39632-w.

[27] Xu HL, Tang W, Du GH, Kokudo N. Targeting apoptosis pathways in cancer with magnolol and honokiol, bioactive constituents of the bark of Magnolia officinalis. Drug Discoveries & Therapeutics. 2011; 5: 202–210. https://doi.org/10.5582/ddt.2011.v5.5.202.

[28] Engeland K. Cell cycle regulation: p53-p21-RB signaling. Cell Death and Differentiation. 2022; 29: 946–960. https://doi.org/10.1038/s41418-022-00988-z.

[29] Rodríguez-Vargas JM, Ruiz-Magaña MJ, Ruiz-Ruiz C, Majuelos-Melguizo J, Peralta-Leal A, Rodríguez MI, *et al*. ROS-induced DNA damage and PARP-1 are required for optimal induction of starvation-induced autophagy. Cell Research. 2012; 22: 1181–1198. https://doi.org/10.1038/cr.2012.70.

[30] Du L, Mei HF, Yin X, Xing YQ. Delayed growth of glioma by a polysaccharide from Aster tataricus involve upregulation of Bax/Bcl-2 ratio, activation of caspase-3/8/9, and downregulation of the Akt. Tumour Biology. 2014; 35: 1819–1825. https://doi.org/10.1007/s13277-013-1243-8.

[31] She EX, Hao Z. A novel piperazine derivative potently induces caspase-dependent apoptosis of cancer cells via inhibition of multiple cancer signaling pathways. American Journal of Translational Research. 2013; 5: 622–633.

[32] Ewings KE, Wiggins CM, Cook SJ. Bim and the pro-survival Bcl-2 proteins: opposites attract, ERK repels. Cell Cycle. 2007; 6: 2236–2240. https://doi.org/10.4161/cc.6.18.4728.

[33] Das A, Banik NL, Patel SJ, Ray SK. Dexamethasone protected human glioblastoma U87MG cells from temozolomide induced apoptosis by maintaining Bax:Bcl-2 ratio and preventing proteolytic activities. Molecular Cancer. 2004; 3: 36. https://doi.org/10.1186/1476-4598-3-36.

[34] Zhang LL, Zhang J, Gao S, Luo RM, Li YL. Effect of DJ-1-regulated PI3K/Akt Signaling Pathway on Mitochondrial Apoptosis during Storage in Qinchuan Beef. Journal of Future Foods. 2025. https://doi.org/10.1016/J.JFUTFO.2024.12.014. (in press)

[35] Zhang YH, Wu YL, Tashiro SI, Onodera S, Ikejima T. Reactive oxygen species contribute to oridonin-induced apoptosis and autophagy in human cervical carcinoma HeLa cells. Acta Pharmacologica Sinica. 2011; 32: 1266–1275. https://doi.org/10.1038/aps.2011.92.